ICES Journal of Marine Science

ICES Journal of Marine Science (2018), 75(5), 1803–1812. doi:10.1093/icesjms/fsy029

Original Article

A method to automatically detect fish aggregations using horizontally scanning sonar

Sindre Vatnehol*, Hector Peña, and Nils Olav Handegard

Institute of Marine Research, Postboks 1870 Nordnes, 5817 Bergen, Norway

**Corresponding author: tel: +47 900 79 376; e-mail: sindre.vatnehol@imr.no.*

Vatnehol, S., Peña, H., and Handegard, N. O. A method to automatically detect fish aggregations using horizontally scanning sonar. – ICES Journal of Marine Science, 75: 1803–1812.

Received 21 November 2017; revised 23 January 2018; accepted 9 February 2018; advance access publication 24 April 2018.

Pelagic fishes are a major source of protein and unsaturated fatty acids, and robust management is critical to avoid overfishing. Fisheries management is often supported by indices from scientific acoustic-trawl surveys, where vertically aligned echo sounders and trawl samples are used to provide an estimate of abundance. Survey biases may be introduced when fish are located near the sea surface or if they avoid the survey vessel. Horizontally scanning acoustic equipment, such as fish-detection sonars, have been proposed as a method to quantify such biases; however, manual interpretation of the data hamper further development. An automated method for identifying fish aggregations within large volumes of sonar data has been developed. It exploits the fact that near-stationary targets, i.e. a fish school, have distinct patterns through the data. The algorithm is not instrument specific, and was tested on data collected from several acoustic-trawl surveys in the Norwegian Sea. The automatic algorithm had a similar performance to manual interpretation, and the main cause of discrepancies was aggregations overlooked in the manual work. These discrepancies were substantially reduced in a second round of manual interpretation. We envision that this method will facilitate a labour efficient and more objective analysis of sonar data and provide information to support fisheries management for pelagic fish.

Keywords: automatic fish detection, interpretation, marine acoustics, pattern recognition, pelagic fish management, sonar, survey bias.

Introduction

Highly efficient fishing fleets around the world target pelagic fishes such as herring, pollock, mackerel, sprat, and anchovy(Watson *et al.*, 2006), which are major components of several ecosystems and an important source of proteins for human consumption. A robust system for managing these stocks is needed for sustainable fisheries, and scientific surveys are often conducted to support these fisheries. The advantage of these surveys, as opposed to catch sampling and catch per unit effort data, is that they are independent from the fishery itself. Pelagic fish stocks are typically surveyed using acoustic-trawl surveys (MacLennan, 1990), resulting in independent indices of abundance that are used in the assessment models.

Standard acoustic-trawl surveys commonly use net sampling and vertically aligned echo sounders to provide independent estimates of abundance (Simmonds and MacLennan, 2005). However, in some years, the estimates from the surveys are mismatching either the assessment or its own internal consistency (ICES, 2016). This inconsistency is often referred to as "year effects" by assessment biologists, which may be more precisely referred to as annual bias. These biases may be caused by many factors, but a variable amount of fish in the upper blind zone (Scalabrin *et al.*, 2009; Totland *et al.*, 2009) and different behavioural reactions (avoidance) (Hjellvik *et al.*, 2008; De Robertis and Handegard, 2013) between years have been proposed as possible explanations. To resolve this, horizontally observing fisheries sonars have been proposed as a tool to augment the traditional echo sounder methodology since these sonars may have the capability to quantify these biases (Goncharov *et al.*, 1989; Misund and Aglen, 1992; Mayer *et al.*, 2002).

Fishery sonars have been proposed as an important tool for fisheries management for decades (Brehmer *et al.*, 2006); and

have been used to detect migration patterns (Hafsteinsson and Misund, 1995; Trygonis *et al.*, 2009; Peraltilla and Bertrand, 2014), map schooling fish near the surface (Misund *et al.*, 1996a), used to detect fish avoidance reactions (Misund *et al.*, 1996b; Soria *et al.*, 1996; Peña *et al.*, 2013), and used to evaluate single school size and fish abundance (Misund, 1993; Tang *et al.*, 2006; Nishimori *et al.*, 2009; Tenningen *et al.*, 2015). All these represent different techniques that, when applied to whole time series and included into the assessment models, can increase both the accuracy and precision of the stock assessment, i.e. by quantifying fish in the blind zone. Despite their potential, the application of fisheries sonars in standard fisheries management has been limited.

A major obstacle, for integrating sonar as a scientific tool, is that processing of sonar data requires substantial manual input, and to realise the potential of the sonar this needs to be almost completely automated. Methods have been developed to automate conventional vertical multi-frequency echo sounder data processing, where these methods utilize the frequency content, signal amplitude and object shape (Kloser *et al.*, 2002; Korneliussen and Ona, 2003; Proud *et al.*, 2015; Korneliussen *et al.*, 2016). The size, distribution, and area density of aggregations are typically quantified by integrating the acoustic energy recorded by the echo sounder, a technique called echo integration (Dragesund and Olsen, 1965; Scherbino and Truskanov, 1966).

Fisheries sonars, with a single frequency, do not have the same coverage in the frequency domain as multi-frequency echo sounder systems, but they do provide better spatial coverage. Current sonar-data processing-methods typically use "dilation-erosion" type image-processing techniques, where neighbouring pixels exceeding a threshold level are connected (Haralick *et al.*, 1987; Reid and Simmonds, 1993; Barange, 1994; Trygonis *et al.*, 2009). Objects with inadequate size, shape and echo amplitude are often excluded, where these criteria are continuously adjusted by experienced users. Systems that use video screen capturing from fisheries sonar have been developed and used for automatic registration of bluefin tuna school echoes (Uranga *et al.*, 2017). These methods search only for fish aggregations in the range and angle domain within each individual ping; hence, patterns in the time domain are not recognized. Assuming a moving vessel and a near-stationary aggregation of fish, multiple sonar images of the fish aggregation would form a pattern in the time, range and angle domain that can be exploited (cf. Figure 1). Search algorithms that exploit this would potentially improve categorization of fish aggregations, and enable efficient data processing of fisheries sonar data.

The objectives of this paper are to (i) provide a robust method to automatically identify fish aggregations from background noise utilizing the patterns in the data (Figure 1), and (ii) demonstrate the efficacy of the method by comparing the output of the automated algorithm to manually interpreted data sets by an experienced user.

Material and methods

Fisheries sonars come in various configurations, but they typically have a cylindrical transducer that emits an acoustic signal, which is usually focused into a horizontal fan covering 360° (Blomberg *et al.*, 2012). If the propagating sound wave encounters an object with a different acoustic impedance to water, such as fish, sound is scattered back towards the transducer (Foote, 1980). Multiple acoustic beams are formed to obtain angular resolution (Sherman and Butler, 2007). The orientation of the beams typically alternates between two configurations, known as the *horizontal* and the *vertical* mode. In the horizontal and vertical mode the fan of beams is arranged in a horizontal circle and a vertically aligned sector, respectively (Tang *et al.*, 2006). The magnitude of the echo is recorded by the sonar for each ping, beam and range interval and converted into volume backscattering coefficients (s_v) (Macaulay *et al.*, 2016).

Acoustic data

Sonar data have been stored during several acoustic-trawl surveys from IMR (Norwegian Institute of Marine Research) monitoring programs, including surveys targeting Atlantic mackerel (*Scomber scombrus*) and Norwegian spring spawning herring (*Clupea harengus*). From these data, 15 cases were selected (Table 1), each representing different challenges for automated data processing. The challenges includes; (i) many small scattered schools of fish, (ii) large layers covering most of the fan and often interpreted as noise or surface reverberation, (iii) actual surface reverberation (cf. Figure 1). Each test case consists of data collected over 4 nautical miles, with the exception of case 7 (the ping repetition interval was substantially longer, and the distance was extended to 12 nautical miles to compensate).

Equipment description

The fisheries sonars available during the acoustic-trawl surveys were the Simrad SH90, SX90, or SU90 (Simrad, 2007, 2013, 2015). The sonar operation frequency and recording range varied among surveys (Table 1). The sampling resolution along the

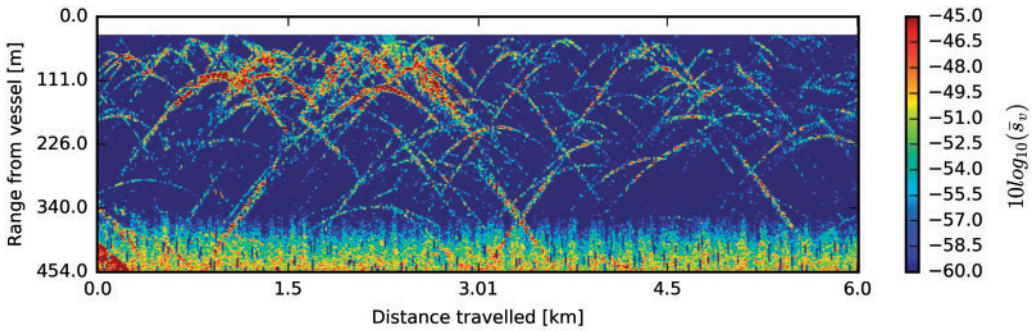

Figure 1. Examples of patterns in sonar data generated from fish aggregations. The data is projected onto a 2D-echogram, with range from the vessel and time/distance travelled as *y*- and *x*-axis, respectively, and averaged across the 64 beams. When the surveying vessel move with a constant velocity, the echo traces from fishes aggregated into schools are seen as parabolic shapes. Noise from surface reverberation is visible approximately between 340 and 450 m range from the vessel.

Table 1. Summary of all test cases that were used.

Test case	Start time Start location	Experienced difficulty	Vessel name	Sonar model	Beam elevation angle [degree]	Signal frequency [kHz]	Sonar detection range [m]	Species	Specific challenge
Case 1	2016-05-04, 09: 33: 00 UTC 62.898737°N 1.753440°E	Hard	F/V Kings Bay	SU90	10	30	300	*Clupea harengus*	Small scattered schools
Case 2	2016-05-05, 20: 24: 30 UTC 62.98269°N 0.989955°E	Moderate	F/V Kings Bay	SU90	10	30	300	*Clupea harengus*	Large scattered schools
Case 3	2016-05-09, 05: 25: 50 UTC 64.262712°N 4.877732°E	Easy	F/V Kings Bay	SU90	10	30	300	*Clupea harengus*	Few large schools
Case 4	2016-05-09, 07: 30: 14 UTC 64.223133°N 4.786473°E	Moderate	F/V Kings Bay	SU90	10	30	300	*Clupea harengus*	Large and dense schools
Case 5	2016-05-10, 20: 05: 10 UTC 64.194127°N 2.457392°E	Easy	F/V Kings Bay	SU90	10	30	300	*Clupea harengus*	Large and dense schools
Case 6	2016-05-03, 13: 56: 00 UTC 62.832320°N 1.807002°E	Hard	F/V Kings Bay	SU90	10	30	300	*Clupea harengus*	Small scattered schools
Case 7*	2012-11-21, 00: 53: 02 UTC 68.64811°N 7.315854°E	Easy	R/V G. O. Sars	SX90	8	26	1200	*Clupea harengus*	Large schools
Case 8	2017-05-14, 17: 50: 00 UTC 64.882202°N 10.290623°W	Moderate	F/V Vendla	SX90	8	26	450	*Clupea harengus*	Small scattered schools + surface reverberation
Case 9	2017-05-14, 21: 11: 00 UTC 64.914240°N 10.160350°W	Hard	F/V Vendla	SX90	8	26	450	*Clupea harengus*	Small scattered + layer
Case 10	2017-05-16, 18: 44: 00 UTC 64.869568°N 11.262598°W	Hard	F/V Vendla	SX90	8	26	450	*Clupea harengus*	Layer
Case 11	2017-05-19, 16: 12: 23 UTC 64.872675°N 5.829930°W	Moderate	F/V Vendla	SX90	8	26	450	*Clupea harengus*	Scattered schools and layer
Case 12	2017-05-20, 18: 24: 23 UTC 64.841678°N 2.607665°W	Hard	F/V Vendla	SX90	8	26	450	*Clupea harengus*	Scattered schools
Case 13	2017-07-17, 17: 26: 20 UTC 66.980027°N 1.032173°W	Easy	F/V Kings Bay	SH90	8	114	450	*Scomber scombrus*	Large schools
Case 14	2017-07-22, 19: 23: 20 UTC 69.023990°N 5.539918°W	Easy	F/V Kings Bay	SH90	8	114	450	*Scomber scombrus*	Large schools
Case 15	2013-05-12, 09: 44: 57 UTC 60.594448°N 2.756398°E	Moderate	F/V Eros	SX90	10	26	450	*Clupea harengus*	Small scattered schools + surface reverberation

The difficulty level of the first semi-automatic interpretation is given, along with sonar model, targeted species, beam elevation angle, sonar operation frequency, recording range, start time and start location. The asterisk in case 7 indicate the travelled distance was increased from 4 to 12 nautical miles to compensate for a substantially longer ping repetition interval than the other cases.

beam is independent of the sonar model, frequency, and pulse length, and is approximately 0.37 m.

The sonars have a cylindrical transducer and generate 64 beams that receives backscattered energy. The direction of the nth beam is ϕ_n and θ_n for azimuth and elevation direction, respectively. n indicate the index of the beam, $n \in [1, 2, \ldots, 64]$. We are only utilizing the horizontal mode, where both ϕ_n and θ_n are fixed; specifically, $\phi_n = \frac{2\pi(n-1)}{64}$ and θ_n is typically between 5 and 10° below the horizontal. The elevation angles for each dataset are specified in Table 1. The nominal beam widths in the horizontal and vertical cross-section are 8.5° and 5.3°, respectively, for the SU90 at 30 kHz, 8.5° and 7.4° for the SX90 on the same frequency, and 8° and 7.5° for the SH90 at 114 kHz.

Semi-automatic process

To evaluate the algorithm's performance, we compared its output to a reference dataset obtained with the IMR's current standard tool for detecting fish aggregations from fisheries sonar: the "Processing system for omnidirectional fisheries sonar" [PROFOS, (Peña *et al.*, 2013)]. PROFOS is a module of the Large Scale Survey System (Korneliussen *et al.*, 2006). The software automatically "grow" schools ping by ping, but the software does require manual intervention and we refer to the method as the semi-automatic approach.

Several PROFOS parameters (Table 2) are adjusted during processing to optimize detection of fish-aggregations. Typically, when aggregations were left undetected by PROFOS or false detections were present, and this was observed by the user, the detection parameters were adjusted and the data re-interpreted. If the combination of parameters still caused false detection or failed to detect a visible aggregation, it was manually edited using a drawing tool in the software. Air-bubbles generated by the propeller produce relatively high backscattered energy, and were often proposed as candidates for fish aggregation. To avoid this, a region in the aft-direction was excluded from the analysis. These actions were repeated until the operator was satisfied with the interpreted result. This complete exercise is coined the *first interpretation*.

After the first interpretation of the sonar data, the specific challenge in processing each test case was noted (cf. Table 1). In addition, the difficulty was classified into simple, moderate or hard based on the time it took to perform the analysis. "Easy" involved almost no manual intervention and the time needed to interpret the output was typically <2 s per ping. For moderate and hard the times were typically between 2 and 4 s/ping, and >4 s/ping, respectively.

Table 2. Summary of the standard parameters used in the PROFOS semi-automatic procedure.

Parameter	Units	Nominal parameter	Parameter used
Adaptive threshold	[dB]	8	5–12
Max ping from seed	–	10	3–10
Max missing pings	–	1	1–4
Min/Max Δs_v	[dB]	2	2
Min surface area	[m^2]	100	10–300
Max surface area	[m^2]	30 000	30 000
Max aspect ratio	–	10	2–20
Min ping count	–	7	3–10

The parameters were adapted to allow visible aggregations to be detected.

The data, interpretation mask, and coordinate system

The sonar data was structured into a 3-dimensional matrix, $\boldsymbol{s_v}$, with the dimensions $[MxNxL]$, where M is the total number of samples along range direction, N is the total number of beams and L is the number of loaded pings. The notation $s_{v,lmn}$ is used to refer to a single element in $\boldsymbol{s_v}$ and indicates the recorded volume backscattering coefficient at the m sample in range, the n beam and the l transmission. A binary mask $\boldsymbol{w}$, with equal dimensions as $\boldsymbol{s_v}$, is defined, where $w_{lmn} = 1$ when the voxel belongs to an aggregation of fish and zero otherwise. Both PROFOS and our method produces this mask, denoted $\boldsymbol{w^P}$ and $\boldsymbol{w^A}$, respectively, for each data set.

A geo-referenced coordinate system, with the vessel location at the beginning of each transect as the origin, is defined (Figure 2). The x-axis is defined to be along the transect line and positive y is toward starboard side. By visualizing $\boldsymbol{s_v}^{\circ}\boldsymbol{w^P}$, where $^{\circ}$ denotes element by element multiplication and assuming the vessel is moving in a straight line with constant speed (typical for surveying vessels), the trajectory of the aggregation is visible as a spiralling parabolic shape (Figure 3).

The coordinates of the pixels in $\boldsymbol{s_v}$ are given by matrix $\boldsymbol{x}$ and $\boldsymbol{y}$, with identical dimensions as $\boldsymbol{s_v}$. The coordinate of $s_{v,lmn}$ is

$$x_{lmn} = x_{mn}^{sonar} + x_l^{vessel} \tag{1}$$

and

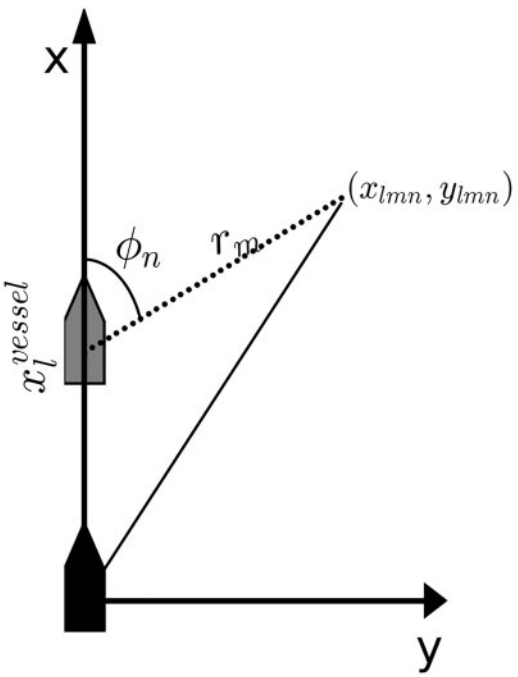

Figure 2. Sketch of the geo-referenced coordinate system with location of the vessel and sonar data pixels. The origin of the coordinate system is at the vessel's location at the start of a transect, black colour. The vessel's location at the lth measurement is shown with a grey colour. The location of a data pixel is given with the spherical coordinates φ_n, θ_n, and r_m when referred to the vessel location. In the global coordinate system, the data pixel location is x_{lmn} and y_{lmn}.

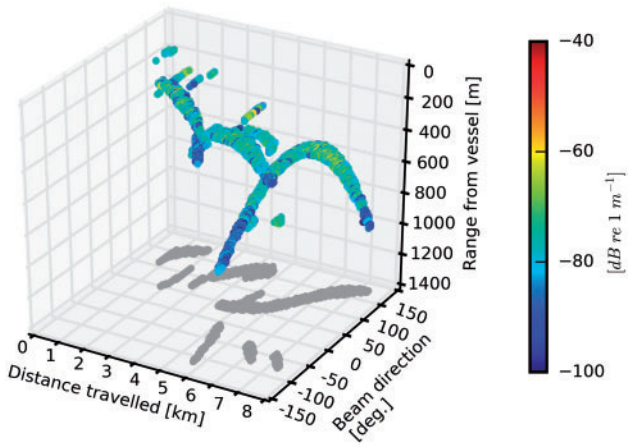

Figure 3. Illustration of interpreted data from test case 7 plotted in time (travelled distance), range and bearing dimension. Z-axis shows the range between the data pixel and the vessel. A beam direction of 0° indicates towards aft, positive angles towards the port side. Grey dots are the projection of data pixels on the *xy*-plane.

$$y_{lmn} = y_{mn}^{sonar}, \tag{2}$$

where x_{mn}^{sonar} and y_{mn}^{sonar} are the coordinates of the $s_{v,lmn}$ data point relative to the vessel's own coordinate system,

$$x_{mn}^{sonar} = r_m \sin\theta_n \cos\phi_n \tag{3}$$

And

$$y_{mn}^{sonar} = r_m \sin\theta_n \sin\phi_n, \tag{4}$$

and x_l^{vessel} is the vessel location along the transect-line. x_l^{vessel} was computed using the distance between the GPS location at the start of the transect and the GPS location of the current measurement.

The search algorithm

To automate the data processing, the spiralling parabolic shape in time, range and bearing space is exploited (Figure 3). In image processing, the location of imperfect lines or shapes can be found using the Hough-transformation (Hough, 1962; Ballard, 1981). Our algorithm has a similar concept, where all s_v values originating a distance R_s from the trajectory line, i.e. the distance from the centre of an aggregation on each ping, are integrated via

$$s_{a_{ij}}^H = \sum_0^R \sum_0^{t_l} \sum_0^{2\pi} w_{ij} s_{v,lmn}, \tag{5}$$

where

$$w_{ij} = \begin{cases} 1 & if \ \sqrt{\left(x_{lmn} - x_{s,ij}\right)^2 + \left(y_{lmn} - y_{s,ij}\right)^2} \\ & \quad \leq \left(R_s + r_m \sin\left(\frac{2\pi}{64}\right)\right) \\ 0 & |\phi_n| > 160^o \ or \ otherwise \end{cases}. \tag{6}$$

$x_{s,ij}$ and $y_{s,ij}$ give the location of the peak of the trajectory in the geo-referenced coordinate system, where i is the index along the travel distance and j the index for distance from the vessel. The $r_m \sin\left(\frac{2\pi}{64}\right)$ term ensures that the two closest beams always are included in the analysis. Similar to the semi-automatic approach, data located in the vessel wake, i.e. $|\phi_n| > 160^o$, are excluded.

The algorithm searches through all data, on both sides of the vessel and along the vessel direction, and develops a search-matrix. This search-matrix is defined as

$$S_a^H = \begin{bmatrix} s_{a,\ 11}^H & \cdots & s_{a,I1}^H \\ \vdots & \ddots & \vdots \\ s_{a,\ 1J}^H & \cdots & s_{a,IJ}^H \end{bmatrix}. \tag{7}$$

If there is a fish aggregation present, the magnitude of $s_{a,ij}^H$ will increase proportionally with the backscattered energy and the duration the fish aggregation is visible through the background noise (Figure 4). Also, importantly, even if the fish aggregation disappears for several pings and reappears (cf. Figure 1), it would still be within the same $s_{a,ij}^H$ and can thus be identified as the same aggregation.

Fish aggregation identification

Removal of background noise data

Prior to estimating $\boldsymbol{w^A}$, the acoustic data need to be processed to remove background noise and surface reverberation. Data containing background noise was removed and excluded from the analysis using

$$s_{a,ij}^H = \begin{cases} s_{a,ij}^H & if \ s_{a,ij}^H \geq n_j * th \\ 0 & otherwise \end{cases}, \tag{8}$$

were n_j is the predicted noise level along the range direction, computed using the median of $s_{a,ij}^H$ along the travel direction, *th* is a threshold parameter.

Removal of false aggregations

The beam pattern of cylindrical transducers, with similar characteristics as the ones used here, includes grating lobes when forming single beams (Sherman and Butler, 2007). When viewing the sonar display, if denser aggregations are within the volume of a grating lobe, the aggregations would then be visible in the direction of the main lobe, i.e. in areas with no fish. Such echoes, coined ghost schools, are visually similar to the echoes of real fish aggregation, but they can be identified as they are always at the same range but rotated approximately 90°, in both directions, relative to the vessel. These ghost schools are usually excluded during manual interpretation. Strictly speaking, this is not a correct approach if the echo integration method is used since the method requires integration over the full beampattern of the sonar. But since this data has been removed, and we want to compare the automatic algorithm to the manual interpretation, we need to remove this data also from the automatic algorithm.

The ghost schools can also be automatically identified as they follow a trajectory perpendicular to the real aggregations. By repeating Equations (2–8) twice, adding positive and negative rotation in Equations (4) and (5) sequentially, the ghost schools can be removed using

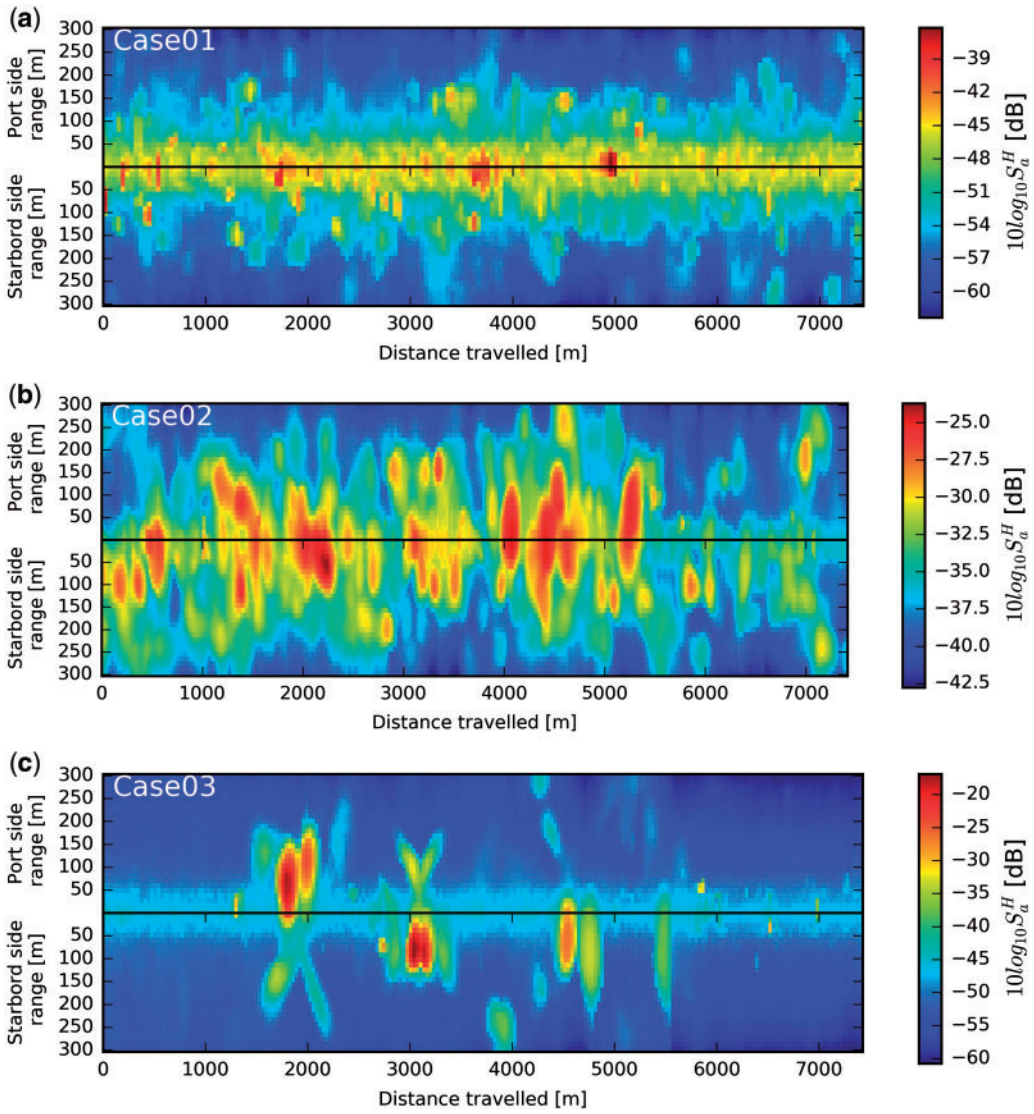

Figure 4. Visualization of the search-matrix for test cases 1–3, where each pixel represents an integration of data around a trajectory line. Top panel is case 1 with a difficulty classified as hard, middle panel is case 2 with moderate difficulty, and lower panel is case 3, which was classified as easy to interpret manually. The *x*-axis is the distance travelled, and *y*-axis is the distance from port and starboard side. The colour scale indicates the magnitude of the accumulated echo energy in log scale.

$$s_{a,ij}^H = \begin{cases} s_{a,ij}^H & \text{if } s_{a,ij}^H - \max\left(s_{a,ij}^{H+\frac{\pi}{2}}, s_{a,ij}^{H-\frac{\pi}{2}}\right) \geq 0 \\ 0 & \text{else} \end{cases}. \quad (9)$$

Here, $s_{a,ij}^{H+\frac{\pi}{2}}$ indicates the search-matrix when a 90° rotation has been added to the beam direction, and $s_{a,ij}^{H-\frac{\pi}{2}}$ when −90° rotation is added.

Removal of surface reverberation and wake bubbles

The sonar system automatically adjusts the beams direction for any offset made by vessel pitch and roll, although this adjustment is often insufficient for larger vessel movements i.e. in bad weather. When the beam elevation angle is near horizontal, the movement of the vessel will cause increased surface reverberation on several beams. The data from these beams are adversely affected and were removed during the semi-automated processing, either by adapting the parameters or manually using the drawing tool.

Manual removal of these echoes was not an option in the automated approach, and we used the vessel's motion reference unit (MRU) to automate the task. A measurement was ignored when

$$w_{mnl}^A = 0 \text{ if } |\Theta_l| > \left(\theta_{e,l} - \frac{\theta_{BW}}{2}\right) \text{ or } |\Phi_l| > \left(\theta_{e,l} - \frac{\theta_{BW}}{2}\right), \quad (10, \text{a})$$

where Θ_l and Φ_l are the recorded vessel pitch and roll angle, respectively, $\theta_{e,l}$ a beam elevation angle and θ_{BW} the vertical beam width. The subscript "l" indicates the lth ping. Although not part of our test scenarios, this filter could also remove data where the sonar operator has set an unfavourable direction of the beams; such as a beam elevation angle less than half the vertical beam width.

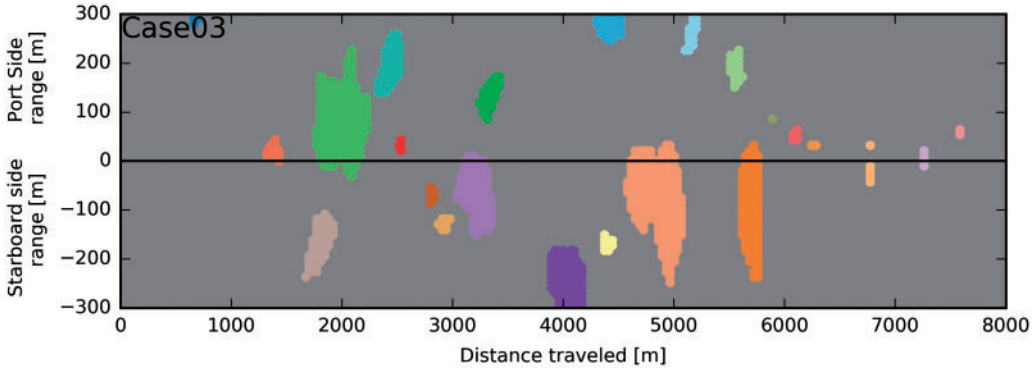

Figure 5. Locations, in the geo-referenced coordinate system, of data classified as fish aggregation in test case 3. Unique fish aggregations are identified using the DBSCAN clustering algorithm. For an easier visual interpretation, random colouring was used on each cluster.

We ignored all data located in the vessel wake when making the search-matrix. These data are also ignored when making $\boldsymbol{w^A}$ via

$$w^A_{lmn} = 0 \;\; if \;\; |\phi_n| > 160^o. \qquad (10, \text{b})$$

Identifying fish aggregations

To identify and count the number of unique aggregations, a density cluster algorithm [DBSCAN, (Ester *et al.*, 1996)] was used on the filtered output of S^H_a (Figure 5). DBSCAN was chosen as no pre-knowledge of number of clusters/aggregations are needed, and it can identify clusters with arbitrary shapes. A single cluster was identified when the cluster size was larger than 1 pixel, and a single pixel was merged with an already existing cluster if the distance to the cluster was less than twice the vessel's travel distance between successive pings. Each cluster is identified with unique locations in the search-matrix, $x_{s,ij}$ and $y_{s,ij}$, and all data pixels where the output of Equation (6) equals one are stored separately for each cluster as a binary mask for further analysis. Two $\boldsymbol{w^A}$ were made by including the mask of all aggregations, and one where ghost schools were excluded.

Sonar echo-integration

The echo integration method is used when evaluating the difference between our algorithm and the semi-automatic approach (MacLennan *et al.*, 2002). The echo integration method is typically applied to the echo sounder data when enumerating fish in acoustic trawl surveys, and we adapt a similar technique on the sonar data, where

$$s_a = \int_0^R \int_0^{t_l} \int_0^{2\pi} \boldsymbol{s_v w^{P/A}} \; d\phi \; dt \; dr. \qquad (11)$$

Here, $\boldsymbol{w^{P/A}}$ indicates that either the interpretation mask made from the PROFOS output or the interpretation mask made from the automatic algorithm is used. The similarity between our algorithm and the semi-automatically protocol was tested by computing the Pearson correlation coefficient (p) for each test case when the acoustic energy was integrated over 200-m bins.

Sensitivity analysis

The algorithm has two variables that influence the output; R_s [Equation (6)] and th [Equation (8)]. To test the sensitivity of these variables, the total sensitivity index [TSI, (*Saltelli et al.*, 2010)] was computed for each of the variables and for each test case.

The algorithm can be described as the function $y = f(R_s, th)$, where y is the algorithm output, [Equation (10)], f being the algorithm as previously described with R_s and th as variables. The total sensitivity index of the variable th is obtained from

$$TSI_{th} = \frac{\frac{1}{2N}\sum_{n=1}^{N}\left(f(R_{s,n}, th_n) - f(R_{s,n}, th^S_n)\right)^2}{V(Y)} \qquad (12, \text{a})$$

and

$$TSI_{R_s} = \frac{\frac{1}{2N}\sum_{n=1}^{N}\left(f(R_{s,n}, th_n) - f(R^S_{s,n}, th_n)\right)^2}{V(Y)} \qquad (12, \text{b})$$

for the variable R_s. N is the number of times the algorithm is initialized with a different set of variables, and $V(Y)$ is the variance of all outputs. $R_{s,n} \in [5,\ 35]$ and $th_n \in [2,\ 31]$ in linear values, where the value used for each initialization is selected using the quasi-random sobol sequence (Morokoff and Caflisch, 1994). The superscript "S" indicates that a second quasi-random sobol sequence was used for these variable inputs.

Results

The method was validated by comparing the automated processed data, using $th = 2.5$ in Equation (8), with data from the semi-automatic process and testing the sensitivity of the output to the parameters.

The accumulated backscattered energy along the vessel track was computed using both $\boldsymbol{w^P}$ and both versions of $\boldsymbol{w^A}$ in 200-m bins (Figure 6) and for the whole data set (Figure 7). This initial comparison revealed, in some cases, large differences between the accumulated backscattered energy. In these cases, the manual interpretation was revisited and corrected in a second inspection, increasing the processing time by 4 s per ping. Note, the difficulty levels indicated in Table 1 were not updated with this additional time. The integration line and the total accumulated energy was re-computed [Equation (11)] using both the original and an updated $\boldsymbol{w^P}$ (Figures 6 and 7). The similarity between the

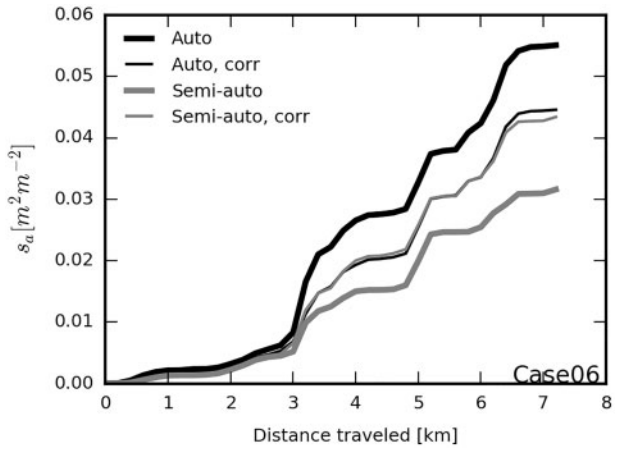

Figure 6. The accumulated echo energy of all data in test case 6 classified as fish aggregation along the vessel's path using either the automatic algorithm (black) or the semi-automatic approach (grey). Corrected data are indicated with thinner lines.

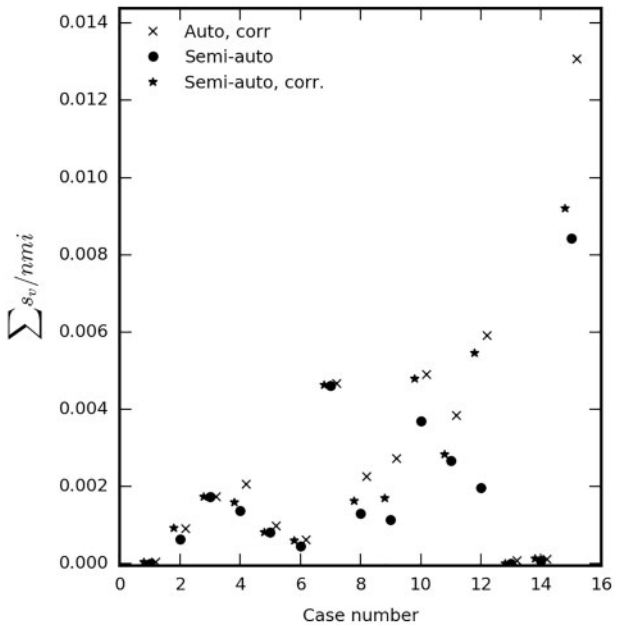

Figure 7. The accumulated s_v, normalized for travel distance, of all data classified as fish aggregation for each test case using the automatic method corrected for ghost schools (cross), the semi-automatic method (circle), and the corrected version of the semi-automatic method (star). Small offset has been added to the *x*-axis values to separate the output from each of the three methods.

automatic algorithm, when ghost schools were removed, and the two versions of $\boldsymbol{w}^{\boldsymbol{P}}$ was computed for each case (Table 3), resulting in a mean Pearson correlation coefficient (p) of 0.76 and 0.85, for the uncorrected and the corrected cases, respectively.

The index of the two total sensitivity coefficients, Equation (12a and b), were computed for each test case (Figure 8). The average between the test cases were 1.5 and 0.1, for $\overline{TSI}_{th}$ *and* $\overline{TSI}_{rs}$, respectively, demonstrating that results of the algorithm is less sensitive to R_S than *th*.

Table 3. The Pearson's correlation coefficient (p) for each test case using the integrated output from both the automatic process and the semi-automatic process.

	Original	Corrected
Case 1	0.6423	0.7711
Case 2	0.5793	0.8551
Case 3	0.9961	0.9961
Case 4	0.9560	0.9700
Case 5	0.9958	0.9958
Case 6	0.8613	0.9805
Case 7	0.8897	0.8904
Case 8	0.7315	0.7839
Case 9	0.6144	0.6812
Case 10	0.4818	0.7560
Case 11	0.8457	0.8435
Case 12	0.6685	0.7170
Case 13	0.8501	0.8578
Case 14	0.7657	0.8786
Case 15	0.7232	0.7913

"Original" indicates the data has been interpreted once with the semi-automatic process, and "corrected" that the interpretation has been revisited. The mean p across data sets was 0.75 for the original and 0.85 for the corrected datasets, where $p \geq 0.8$ indicates a reasonable similarity between the two methods.

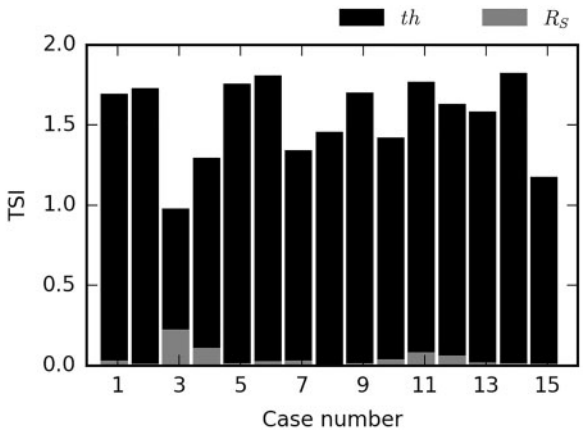

Figure 8. Total sensitivity index for *th* (black bars) and R_s (grey bars), computed for all test cases.

Discussion

We have demonstrated that a pattern through range, time and space domain can be exploited to automatically detect fish aggregations in sonar data. The method was compared with the traditional method (Trygonis *et al.*, 2009; Peña *et al.*, 2013), that only search locally in the space domain and require manual interactions. Integrating all data categorized as fish, using both methods, did revealed discrepancies between the methods (Figures 6 and 7). Overall, the automatic processing algorithm tends to categorise more acoustic energy as fish.

In most of the test cases, the output of the two methods was similar ($p > 0.8$, Table 3), but the traditional algorithm did require substantial manual intervention in several of the cases, i.e. 1, 6, and 9. In addition, a second pass of the semi-automated process reduced the difference between the two methodologies (Figure 7 and Table 3), adding further processing time to obtain

reliable results. The cause of the discrepancy was typically aggregations not detected due to an inadequate setting in the semi-automated process combined with overlooking this in the manual quality control (Table 2). For large aggregation of fish, such as layers extended through the whole detection volume of the sonar, the local search would categorise this as noise. Although the second pass was motivated by a difference between the two methods, the second pass *did* reveal aggregations that were missed (roughly 20–30% of the pings in the worst cases) in the initial run. The excluded vessel wake area can be included in both methods, i.e. ignoring Equation (10.b); however, no notable difference was seen in the results when including this area. Therefore, we have concluded that the traditional algorithm does not have the necessary consistency as it is subject to the experience of the user and time invested to process the data. In contrast, the fully automatic algorithm will always, unless the input variables are altered, produce the same result for each initialization.

The sensitivity was dominated by the threshold level (th) (Figure 8), and a procedure to set the parameters is needed. Ideally, the value of the variables should be set by minimizing the differences between the semi-automatic and the automated process, but the semi-automated method was too inconsistent for such an approach. Instead, we propose to use the approach we used when evaluating the method: First run a pass with the automated method on a subset of the data, then manually review and update the interpretation, and use the reviewed set as basis for the selection of the parameters on the rest of the data.

We have demonstrated that the automated algorithm outperforms the current semi-automatic operation on our acoustic-trawl surveys in two aspects. First, the automatic algorithm is more consistent. This result is important since consistency is imperative when tracking a population over time and space. Second, our algorithm will significantly reduce processing time. With a sonar ping interval of once per second, roughly 16 continuous weeks is needed to thoroughly process 2 weeks of data. In contrast, automatic algorithm allows real time processing. For research surveys, this time would be better spent to monitor the performance of the automated method and improve parameterization of the method.

The core of the method, as it has been described here, utilizes patterns of stationary aggregations when the vessel is moving in straight lines. If the vessel course is changed, i.e. when circumnavigating single aggregations of fish, a search-matrix can still be developed by integrating all backscattering data originated at specific locations in a geo-reference coordinate system. The same procedure to isolate aggregations form the search-matrix can then be applied.

Some biases, such as fish avoidance and the blind zone (Soria *et al.*, 1996; Scalabrin *et al.*, 2009; Totland *et al.*, 2009; De Robertis and Handegard, 2013; Peña *et al.*, 2013) ,which are thought to be major contributors on the stock assessment's total uncertainty, are measurable using these sonars. The avoidance behaviour of Norwegian spring spawning herring is estimated to contribute 16.5–41% of the total uncertainty (Løland *et al.*, 2007). Timeseries with interpreted sonar data can, in this context, either as an independent estimate or as a supplement to the echo sounder estimates, be used to quantify if the blind zone or avoidance behaviour is significantly different between years, time of the year, and location. Also, processed sonar data can yield insights into temporal and spatial variability of grouping behaviour and aggregation in terms of density, size and distance between aggregations.

Conclusion

A method for automatic detection of fish aggregations within fisheries sonar data has been developed. The algorithm can be run with very limited user intervention and is thus much more efficient and more objective than the traditional semi-automatically data processing procedures. We envision that this approach will enable us to test and validate fisheries sonar as a major tool on acoustic trawl surveys.

Acknowledgements

We thank editor David Demer and two anonymous reviewers for comments on the manuscript. We also thank the captain and crew on F/V Kings Bay, F/V Vendla, R/V G. O. Sars, and F/V Eros for their expertise and dedication while collecting the data for this paper.

References

Ballard, D. H. 1981. Generalizing the Hough transform to detect arbitrary shapes. Pattern Recognition, 13: 111–122.

Barange, M. 1994. Acoustic identification, classification and structure of biological patchiness on the edge of the Agulhas Bank and its relation to frontal features. South African Journal of Marine Science, 14: 333–347.

Blomberg, A. E. A., Austeng, A., and Hansen, R. E. 2012. Adaptive beamforming applied to a cylindrical sonar array using an interpolated array yransformation. IEEE Journal of Oceanic Engineering, 37: 25–34.

Brehmer, P., Lafont, T., Georgakarakos, S., Josse, E., Gerlotto, F., and Collet, C. 2006. Omnidirectional multibeam sonar monitoring: applications in fisheries science. Fish and Fisheries, 7: 165–179.

De Robertis, A., and Handegard, N. O. 2013. Fish avoidance of research vessels and the efficacy of noise-reduced vessels: a review. ICES Journal of Marine Science, 70: 34–45.

Dragesund, O., and Olsen, S. 1965. On the possibility of estimating year-class strength by measuring echo-abundance of 0-group fish. Fiskeridirektoratets Skrifter: Serie Havundersøkelser, 13: 47–75.

Ester, M., Kriegel, H. P., Sander, J., and., and Xu, X. 1996. A density-based algorithm for discovering clusters in large spatial databases with noise. *In* Proceedings of the 2nd International Conference on Knowledge Discovery and Data Mining, pp. 226–231.

Foote, K. G. 1980. Importance of the swimbladder in acoustic scattering by fish: a comparison of gadoid and mackerel target strengths. The Journal of the Acoustical Society of America, 67: 2084–2089.

Goncharov, S., Borisenko, E., and Pyanov, A. 1989. Jack mackerel schools' defence reaction to a surveying vessel. Proceedings of the Institute of Acoustic, 11: 74–78.

Hafsteinsson, M., and Misund, O. 1995. Recording the migration behaviour of fish schools by multi-beam sonar during conventional acoustic surveys. ICES Journal of Marine Science, 52: 915–924.

Haralick, R. M., Sternberg, S. R., and Zhuang, X. 1987. Image analysis using mathematical morphology. IEEE Transactions on Pattern Analysis and Machine Intelligence, 9: 532–550.

Hjellvik, V., Handegard, N. O., and Ona, E. 2008. Correcting for vessel avoidance in acoustic-abundance estimates for herring. ICES Journal of Marine Science, 65: 1036–1045.

Hough, P. V. C. 1962. Method and means for recognizing complex patterns. US Patent 3, 069, 654, 21: 225–231. http://www.google.com/patents/US3069654.

ICES. 2016. Report of the Working Group on Widely Distributed Stocks (WGWIDE), 31 August to 6 September 2016. ICES HQ, Copenhagen, Denmark. ICES Document CM 2016/ACOM: 16, pp. 1-506.

Kloser, R. J., Ryan, T., Sakov, P., Williams, A., and Koslow, J. A. 2002. Species identification in deep water using multiple acoustic

frequencies. Canadian Journal of Fisheries and Aquatic Sciences, 59: 1065–1077.

Korneliussen, R. J., and Ona, E. 2003. Synthetic echograms generated from the relative frequency response. ICES Journal of Marine Science, 60: 636–640.

Korneliussen, R. J., Ona, E., Eliassen, I., Heggelund, Y., Patel, R., Godø, O. R., Giertsen, C., *et al.* 2006. The Large Scale Survey System-LSSS. *In* Proceedings of the 29th Scandinavian Symposium on Physical Acoustics, Ustaoset 29 January to 1 February 2006.

Korneliussen, R. J., Heggelund, Y., Macaulay, G. J., Patel, D., Johnsen, E., and Eliassen, I. K. 2016. Acoustic identification of marine species using a feature library. Methods in Oceanography, 17: 187–205.

Løland, A., Aldrin, M., Ona, E., Hjellvik, V., and Holst, J. C. 2007. Estimating and decomposing total uncertainty for survey-based abundance estimates of Norwegian spring-spawning herring. ICES Journal of Marine Science, 64: 1302–1312.

Macaulay, G. J., Vatnehol, S., Gammelsæter, O. B., Ona, E., and Pena, H. 2016. Practical calibration of ship-mounted omni-directional fisheries sonars. Methods in Oceanography, 17: 206–220.

MacLennan, D. N. 1990. Acoustical measurement of fish abundance. The Journal of the Acoustical Society of America, 87: 1–15.

MacLennan, D. N., Fernandes, P. G., and Dalen, J. 2002. A consistent approach to definitions and symbols in fisheries acoustics. ICES Journal of Marine Science, 59: 365–369.

Mayer, L., Li, Y., and Melvin, G. 2002. 3D visualization for pelagic fisheries research and assessment. ICES Journal of Marine Science, 59: 216–225.

Misund, O. A., and Aglen, A. 1992. Swimming behaviour of fish schools in the North Sea during acoustic surveying and pelagic trawl sampling. ICES Journal of Marine Science, 49: 325–334.

Misund, O. A. 1993. Abundance estimation of fish schools based on a relationship between school area and school biomass. Aquatic Living Resources, 6: 235–241.

Misund, O. A., Aglen, A., Hamre, J., Ona, E., Rottingen, I., Skagen, D., and Valdemarsen, J. W. 1996a. Improved mapping of schooling fish near the surface: comparison of abundance estimates obtained by sonar and echo integration. ICES Journal of Marine Science, 53: 383–388.

Misund, O. A., Øvredal, J. T., and Hafsteinsson, M. T. 1996b. Reactions of herring schools to the sound field of a survey vessel. Aquatic Living Resources, 9: 5–11.

Morokoff, W. J., and Caflisch, R. E. 1994. Quasi-random sequences and their discrepancies. SIAM Journal on Scientific Computing, 15: 1251–1279.

Nishimori, Y., Iida, K., Furusawa, M., Tang, Y., Tokuyama, K., Nagai, S., and Nishiyama, Y. 2009. The development and evaluation of a three-dimensional, echo-integration method for estimating fish-school abundance. ICES Journal of Marine Science, 66: 1037–1042.

Peña, H., Handegard, N. O., and Ona, E. 2013. Feeding herring schools do not react to seismic air gun surveys. ICES Journal of Marine Science, 70: 1174–1180.

Peraltilla, S., and Bertrand, S. 2014. In situ measurements of the speed of Peruvian anchovy schools. Fisheries Research, 149: 92–94.

Proud, R., Cox, M. J., Wotherspoon, S., and Brierley, A. S. 2015. A method for identifying Sound Scattering Layers and extracting key characteristics. Methods in Ecology and Evolution, 6: 1190–1198.

Reid, D. G., and Simmonds, E. J. 1993. Image analysis techniques for the study of fish school structure from acoustic survey data. Canadian Journal of Fisheries and Aquatic Sciences, 50: 886–893.

Saltelli, A., Annoni, P., Azzini, I., Campolongo, F., Ratto, M., and Tarantola, S. 2010. Variance based sensitivity analysis of model output. Design and estimator for the total sensitivity index. Computer Physics Communications, 181: 259–270.

Scalabrin, C., Marfia, C., and Boucher, J. 2009. How much fish is hidden in the surface and bottom acoustic blind zones? ICES Journal of Marine Science, 66: 1355–1363.

Scherbino, M., and Truskanov, M. 1966. Determination of fish concentration by means of acoustic apparatus. ICES Document CM 1966/F3:6.

Sherman, C. H., and Butler, J. L. 2007. Transducers and Arrays for Underwater Sound. Springer, New York. 612 pp.

Simmonds, J., and MacLennan, D. 2005. Fisheries Acoustics. Chapman & Hall, London. 325 pp.

Simrad, 2007. Operator Manual SX90, Fish Finder Sonar. 307672/Rev a, Horten, Norway.

Simrad, 2013. Operator Manual SH90, Fish Finder Sonar. Simrad as, 307672/Rev a, Horten, Norway.

Simrad, 2015. Operator Manual SU90, Fish Finder Sonar. Simrad as, 307672/Rev a, Horten, Norway.

Soria, M., Fréon, P., Gerlotto, F. F., Fréon, P., and Gerlotto, F. F. 1996. Analysis of vessel influence on spatial behaviour of fish schools using a multi-beam sonar and consequences for biomass estimates by echo-sounder. ICES Journal of Marine Science, 53: 453–458.

Tang, Y., Iida, K., Mukai, T., and Nishimori, Y. 2006. Estimation of fish school volume using omnidirectional multi-beam sonar: scanning modes and algorithms. Japanese jJurnal of Applied Physics, 45: 4868–4874.

Tenningen, M., Peña, H., and Macaulay, G. J. 2015. Estimates of net volume available for fish shoals during commercial mackerel (Scomber scombrus) purse seining. Fisheries Research, 161: 244–251.

Totland, A., Johansen, G. O., Godø, O. R., Ona, E., and Torkelsen, T. 2009. Quantifying and reducing the surface blind zone and the seabed dead zone using new technology. ICES Journal of Marine Science, 66: 1370–1376.

Trygonis, V., Georgakarakos, S., and Simmonds, E. J. 2009. An operational system for automatic school identification on multibeam sonar echoes. ICES Journal of Marine Science, 66: 935–949.

Uranga, J., Arrizabalaga, H., Boyra, G., Hernandez, M. C., Goñi, N., Arregui, I., Fernandes, J. A., *et al.* 2017. Detecting the presence-absence of bluefin tuna by automated analysis of medium-range sonars on fishing vessels. PLoS One, 12: e0171382.

Watson, R., Revenga, C., and Kura, Y. 2006. Fishing gear associated with global marine catches: i. Database development. Fisheries Research, 79: 97–102.

Handling editor: David Demer